LBL--27590

DE91 004250

# Displacement Sensors for the Primary Mirror of the W.M. Keck Telescope

R.H. Minor, A.A. Arthur, G. Gabor,
H.G. Jackson, and R.C. Jared
Engineering Division
Lawrence Berkeley Laboratory
University of California
Berkeley, CA 94720

and

T.S. Mast and B.A. Schaefer
Physics Division
Lawrence Berkeley Laboratory
University of California
Berkeley, CA 94720

Primary funding was provided by the California Association for Research in Astronomy. This work was supported in part by the Director, Office of Energy Research, Office of Health and Environmental Research, Physical and Technological Division of the U.S. Department of Energy under Contract No. DE-AC03-76SF00098.

LBL-27590

# Displacement sensors for the primary mirror of the W.M. Keck telescope

R.H. Minor, A.A. Arthur, G. Gabor, H.G. Jackson,
R.C. Jared, T.S. Mast[1] and B.A. Schaefer[1]
Engineering & [1]Physics Divisions, Lawrence Berkeley Laboratory
1 Cyclotron Road, Berkeley, CA 94720

## ABSTRACT

The Primary Mirror of the Keck Observatory Telescope is made up of an array of 36 hexagonal mirror segments under active control. The measurement of the relative orientations of the mirror segments is fundamental to their control. The mechanical and electronic design of the sensors used to measure these relative positions is described along with the performance of the sensors under a variety of tests. In use, the sensors will measure relative positions with a resolution of a few nanometers. This resolution and the low noise, drift and thermal sensitivity of the sensors are adequate to stabilize the primary mirror figure to the precision required for optical and infrared astronomy.

## 1. INTRODUCTION

The primary mirror of the Keck Observatory Telescope is made up of 36 hexagonal mirror segments. The Primary Mirror Support System (PMSS) holds these 36 segments in position allowing the array to act as if it were a single mirror. The Passive Support System supports each mirror segment and controls its rotation in the mirror plane. The Active Control System (ACS) controls the tilt and piston of each segment relative to the other segments. The ACS uses position sensors on the back of the segments to measure their relative positions, control electronics hardware and software to interpret the position data, and actuators to move the segments as commanded. Figure 1 shows the locations of the sensors on the primary mirror array. Sensors are positioned so that the effective sensing locations are offset from the gap between segments and alternated across the gap to give sensitivity to overall focus as well as piston and tilt of the individual segments. The ACS control loop holds the mirrors in a predetermined alignment. That alignment is established during a calibration procedure using images of stars in cameras sensitive to mirror segment alignment. The precision with which the mirror array may be held in alignment depends to a large part on the precision and stability of the sensor. The ACS is more fully described in the paper, "The W.M. Keck Telescope Segmented Mirror Active Control System".[1] The development of the sensor has been previously described in Refs. 2, 3 and 4.

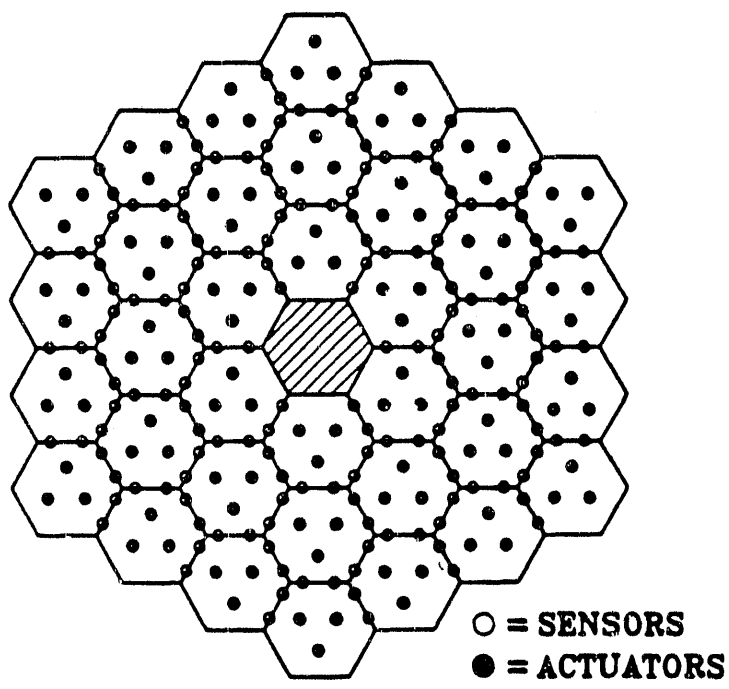


Fig. 1: Primary mirror sensor locations

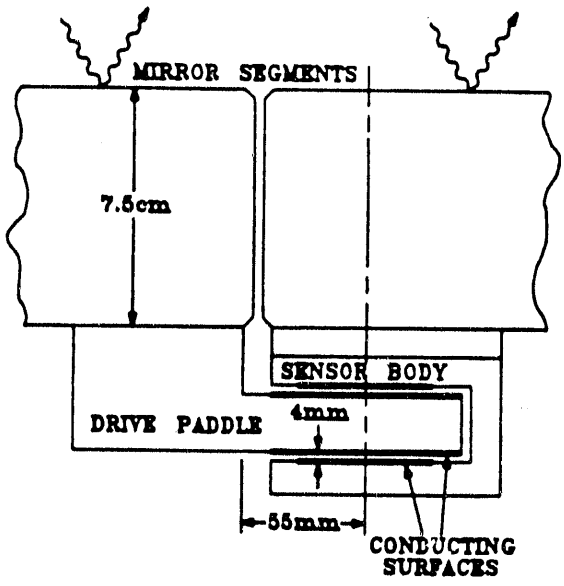


Fig. 2: Sensor cross section

## 2. DESCRIPTION

Figure 2 shows a simplified cross section of a sensor. Figure 3 is a plan view. One half of the sensor is attached to each mirror. The sensor mechanical parts are mounted on the rear of the mirror and do not interfere with the imaging of stars. The drive paddle moves relative to the sensor body when the two segments move relative to each other, changing the spacing of the coated areas that form two sense capacitors. Since the capacitance is proportional to the spacing, the difference in capacitance is proportional to the displacement. The sensor preamplifier/analog-to-digital converter (sensor preamp/ADC) measures this difference in capacitance and produces a digital output proportional to the displacement. This digital output is sent to the ACS control electronics for interpretation.

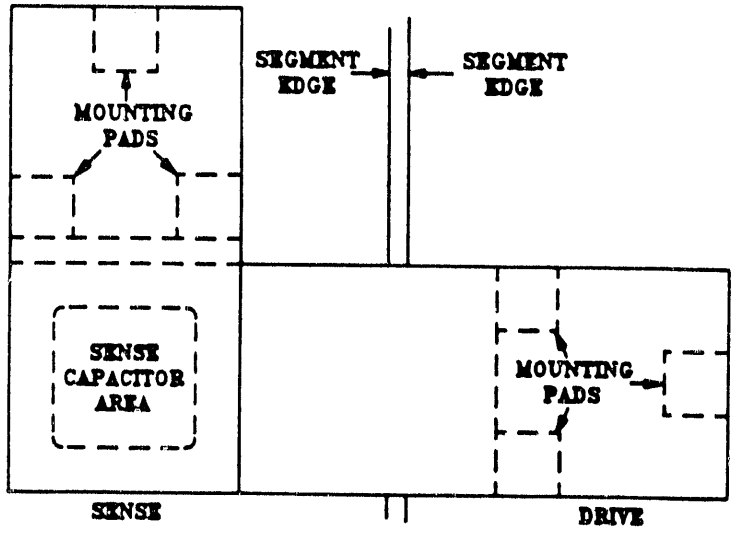


Fig. 3: Sensor plan view

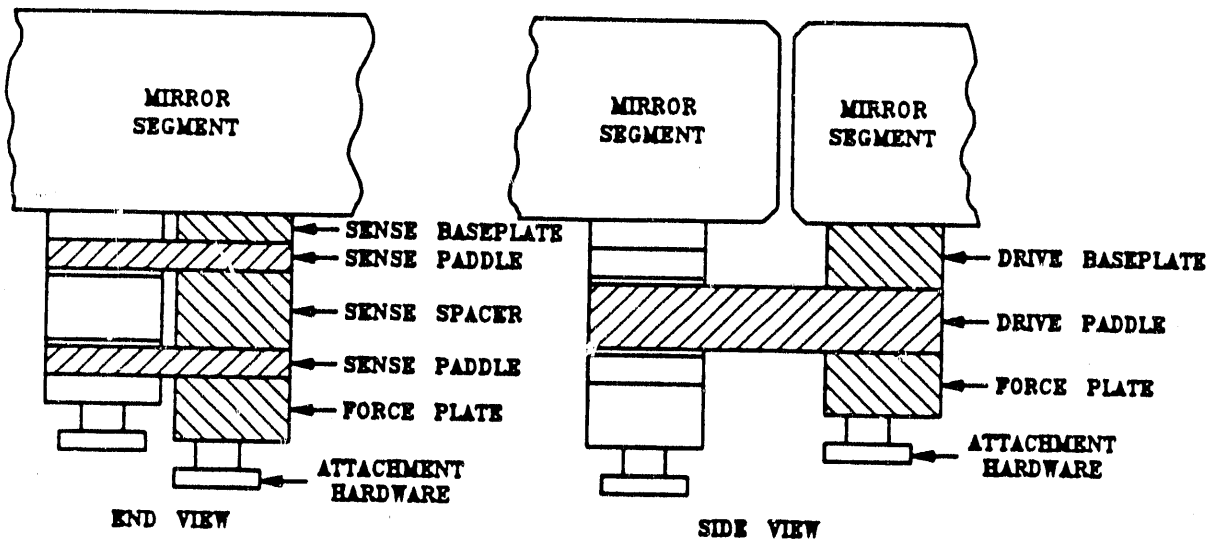


Fig. 4: Sensor components

Figure 4 shows the two halves of a sensor. The drive side consists of three Zerodur parts and attachment hardware (Appendix B). The drive baseplate matches the curvature of the back of the mirror and spaces the drive paddle at the appropriate distance and angle from the mirror front surface. The drive paddle is coated on two sides to form parts of the two sensing capacitors. The sense side consists of a stack of five pieces. The sense baseplate matches the curve of the mirror and spaces the remaining pieces at a standard distance from the optical surface. The two sense paddles are coated to form parts of the sense capacitors and are separated by the sense spacer. The force plates distribute the force of the mounting hardware, holding the stacks in place. Surfaces of the force plates, the sense and drive baseplates, and the sense spacer have been relieved to create three pads at each interface to provide kinematic contact between the pieces. Appendix C describes the fabrication of the Zerodur sensor parts.

The sensor boot encloses the sensor to exclude dirt and to protect the sensor. The field effect transistor preamp (FET preamp) is mounted on the boot as close as possible to the sensing capacitors in order to minimize noise from stray capacitance. The remainder of the sensor preamp/ADC is included in an electronic enclosure (node box) mounted near the mirror.

## 3. PRINCIPLE OF OPERATION

The principle of operation is shown in Fig. 5. The two capacitors formed on the sensor mechanical parts are driven with 20 kHz square waves 180° out of phase. A single master clock generates the 20 kHz which is distributed to all sensor preamp/ADCs.

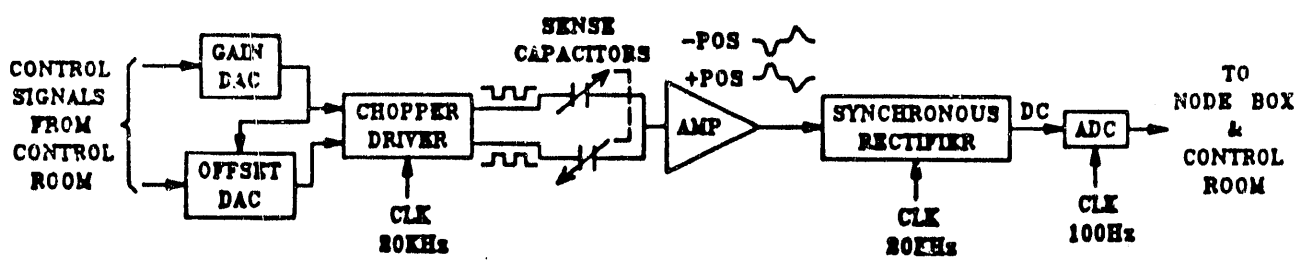


Fig. 5: Block diagram

Square waves are generated by a chopper controlled by the master clock. The amplitudes of the square waves are set by two Digital-to-Analog Converters (DACs) in the preamp/ADC. The gain DAC sets the magnitude of the square wave drive. A local voltage reference holds this level stable. The offset DACs voltage is derived from the gain DAC and adds or substracts to one of the drive signals. Since variation in the fabrication of the sensor parts and the mirror segments may cause a physical offset in the sensor of up to 180 μm when the optical surfaces are in alignment, an electrical offset is applied to keep the sensor output near zero when mirror alignment is achieved. Gain stability requirements are reduced if the sensor output is held near zero. During operation the gain is held constant, but during initial alignment and convergence it is possible to reduce the gain and thereby increase the operating range from the normal ± 12 μm to a full ± 4 mm. Since the offset voltage is derived from the gain voltage the same offset DAC value compensates for the physical offset regardless of sensor gain. Both the gain DAC and the offset DAC are set by the control loop software and may be updated as required as part of compensation of systematic errors in sensor output.

The difference in capacitance caused by drive paddle motion is given by:

$$\Delta C = \frac{2\varepsilon A x}{x_0^2} \cdot \frac{1}{\left[1 - \left(\frac{x}{x_0}\right)\right]^2}$$

where $\varepsilon$ = dielectric constant
$A$ = area of the plates
$x_0$ = centered distance (4mm)
$x$ = displacement of drive paddle

Linearity over the range of ± 12 μm is acceptable even when the sensor is offset by the maximum of 180 μm from center allowed by the mechanical tolerances.

The preamplifier is a charge sensitive amplifier whose conversion of charge to voltage is primarily determined by the feedback capacitor. The preamp consists of a JFET near the sensor and an additional stage in the preamp/ADC itself. The JFET is chosen to minimize low frequency noise. The sense signals are summed at the input to the JFET. Since the drive signals to the two sense capacitors are 180° out of phase, the voltage signal at the output of the preamplifier is proportional to the difference in the value of the two sense capacitors.

Voltage signals are amplified by an amplifier whose gain = 10, filtered by a bandpass amplifier and then synchronously rectified. Additional filtering at 30 Hz is included in the rectifier circuitry. Filtering limits the bandwidth of the preamp/ADC to control aliasing in the ADC and to reduce extraneous noise. The synchronous rectifier generates a DC voltage proportional to the difference in capacitance. A sample and hold with additional filtering holds the DC level for the ADC. The ADC is 12 bits plus sign with an input of ± 5 V for ± 4095 bits. At normal operation 1 bit = 3 nm equivalent motion. Sensor data and control signals are carried to and from the preamp/ADC via a multiplex card in the node box and serial RS-485 links to the control room. Sensor data is read out at a 100 Hz rate.

## 4. DESIGN DETAILS AND PERFORMANCE

The precision and stability of the sensor measurements determine how well the primary mirror will be held in alignment (Appendix A). Sensor readings are influenced by both random and systematic errors including those caused by temperature variation, gravitational deformation, and electronic noise. Systematic errors caused by thermal, gravitational and intersegment motion effects will be corrected by using lookup tables generated during the calibration process. Since these systematic errors are repeatable and show little hysteresis, corrections may be made to at least 10%, and in most cases less than 5% of the effect will remain as a residual error after corrections have been applied. These corrections use data collected during calibration runs using a calibration camera system that will detect the desired alignment of the mirror segments, and record the measured sensor values to be interpreted by the control loop software. Random errors will be seen directly by the control loop software.

The optical budget allots 2.5 nm rms for errors caused by thermal effects on the sensors and on the mirror segments. Thermal effects on the sensors are dominated by the Zerodur material. The Zerodur used for the sensors has a maximum difference in temperature coefficient of $3 \times 10^{-8}$/°C. With a characteristic sensor thickness of 3.5 cm the material alone could contribute a maximum of about 1 nm/°C. Other contributors to sensor thermal effects are variations in spring pressure, attachment hardware metal to glass contact, coating thickness variations, gradients in the temperature coefficient of the Zerodur and temperature gradients at the mirrors. Temperature coefficients of sensors mounted on fixed bases were measured both in a temperature controlled chamber and under the influence of ambient temperature changes. Testing in an oven and in an open environment shows a temperature coefficient for the mechanical part of the sensor of < 1.5 nm/°C. Combined tests of electronics and mechanics show a coefficient of < 2 nm/°C. The Zerodur used for the mirrors has a mean temperature coefficient of $1.0 \times 10^{-8}$/°C with variations of $2.0 \times 10^{-8}$/°C rms. With a thickness of 7.5 cm, a temperature coefficient of 1.5 nm/°C rms may be expected Both the sensor and mirror temperature effects will be corrected to better than 5%.

As the telescope moves from zenith to horizon the physical parts of the sensors will bend in response to gravity. The optical budget allots 9 nm rms for these effects. Since the sensors are not symmetrical in plan, the amount of bending will depend on the orientation of the sensor. Bending takes place both as simple cantilevered beams and as differential column compression and bending. Only the most rudimentary compensation was attempted by sizing the various beams as a function of their length. Gravitational deflections were measured by tilting sensors from the horizontal to the vertical in all orientations that will be encountered on the telescope. Gravitational deflections from horizontal to vertical were measured as 150 nm mean with a maximum of 300 nm. Since these deflections are very repeatable (< 10 nm variation) a correction can be made to better than 5% (7.5 nm rms).

Intersegment lateral motion gives rise to a false indication of longitudinal positioning (see Fig. 6). Since the lateral motion is caused by gravity and temperature effects on the steel support structure, the motion will be repeatable and its effects will be corrected using lookup tables. The tilt of the drive paddle determines the size of the effect. If the drive paddle is perpendicular to the normal to the optical surface above the sense point the error is minimized. Sense baseplate wedge errors have no effect on the performance of the sensor other than affecting the required electrical offset range. Wedge in the segment itself, the mounting location of the baseplate and the fabrication tolerances of the baseplate and drive paddle all contribute to the tilt of the drive paddle. Tilt is held to less than $1.5 \times 10^{-4}$ radian rms giving an expected error of 45 nm rms, which will be corrected to 4.5 nm rms.

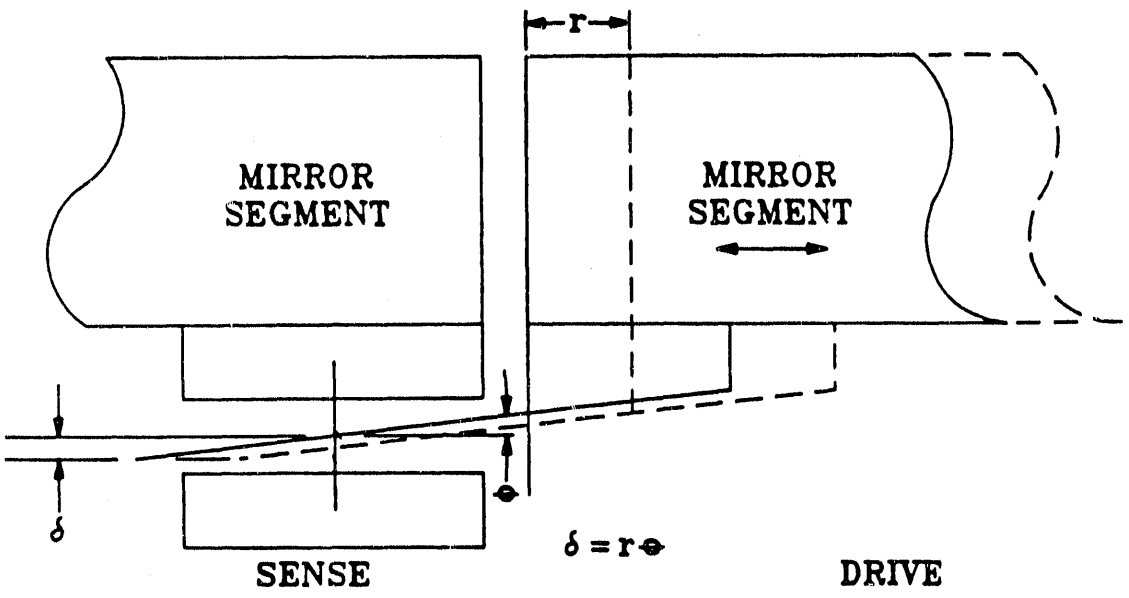


Fig. 6: Sense error from intersegment motion

Intersegment lateral motion also affects the fringe fields of the sensor since the geometry of the sense capacitors is changed. This effect is small. Sensitivity to mechanical alignment was tested by rotating a drive paddle into and out of the gap of a fixed sensor. A motion of 0.3 mm of the drive paddle changes the output < 5 nm.

The time between recalibrations of the mirror array depends on the temporal drift of the sensors. The optical budget allows 6.0 nm/wk for combined mechanical and electronic temporal drift. Electronic drift is < 1 nm/wk. When first assembled, there is an initial exponential mechanical settling of the sensors at the contact pads. Ground Zerodur surfaces at the mounting pads were chosen on the basis of observed settling rates. Contact pads with 10 kg on 2 $cm^2$ with a 5 μm rms surface roughness were chosen for the production sensor. Temporal drift was tested by mounting both halves of sensors to the same rigid block of Zerodur and observing the sensors output under constant temperature conditions and under ambient temperatures. Changes in output not attributable to temperature variations indicate that < 4 nm/wk drift for sensor and electronics combined may be expected after an initial 24 hour settling period.

The optical budget allows 2.5 nm rms for sensor noise. Sensor noise is primarily a function of preamplifier input capacitance and the details of the electronics. The use of a low noise FET front end and the subsequent filtering and synchronous rectification allows the specification to be met comfortably, at < 1 nm rms (30 Hz bandwidth).

Since the sensor electronics are in the telescope dome in close proximity to the mirrors, power consumption and electronic interference were also of concern. Analog signal paths were kept short to minimize noise and interference, and all mirror-to-control-room communication is via serial digital links. Power consumption is < 40 mw for the FET preamp/ADC (at the mirror) and 0.44 W for the preamp/ADC itself.

## 5. CONCLUSION

The low thermal error (< 3 nm/°C), low drift (< 4 nm/wk) and predictable deformation (correctable to better than 7.5 nm rms) of the sensor make it possible for its contribution to the total optical error budget to be set quite low. Sensor errors consume only 9 nm rms of a total alloted budget of 12 nm rms. The sensors' small mass and its low power dissipation allow it to operate without degrading the optical performance directly. Tests prior to installation indicate that the sensors should meet or exceed all the requirements set by the optical budget. When installed in the Keck Observatory Telescope, testing will continue and performance measurements under operating conditions will be made to confirm the performance seen to date.

## 6. ACKNOWLEDGMENTS

We acknowledge the contributions of Dave Pankow of Space Sciences for his assistance with the mechanical design and Will Lawrence, Tom Gee and Zigmunt Wieteska of Lawrence Berkeley Laboratory for their prototype fabrication work. Primary funding was provided by the California Association for Research in Astronomy. This work was supported by the Director's Office of Energy Research, Office of Health and Environmental Research, U.S. Department of Energy under Contract No. DE-AC03-76SF00098. Reference to a company or product name does not imply approval or recommendation of the product by the University of California or the U.S. Department of Energy to the exclusion of others that may be suitable.

## 7. REFERENCES

1. R.C. Jared et al, "The W.M. Keck Telescope Segmented Mirror Active Control System," these proceedings.

2. T.S. Mast, G. Gabor and J.E. Nelson, "Edge Sensors for a Segment Mirror," S.P.I.E. Proc., 444, 297 (1983).

3. H.G. Jackson and T.T. Shimizu, "Position Sensor Electronics for the Ten Meter Telescope," Keck Observatory Tech. Note, No.244 (1987).

4. T.S. Mast and R. Cohen, "Displacement Sensors: Control and Software," Keck Observatory Tech. Note, No.240 (1988).

## APPENDIX A

Specifications and Requirements

Sensor readings are influenced by both random and systematic errors arising from the effects of temperature, gravitational deformation and electronic noise. Performance requirements for the sensors are derived from the overall optical error budget. These are given as:

**OPTICAL BUDGET (after lookup-table correction)**

| | |
|---|---|
| sensor thermal effects | 2.5 nm rms |
| sensor gravitational effects | 9.0 nm rms |
| sensor intersegment motions | 4.6 nm rms |
| sensor temporal drift | 6.0 nm/wk |
| sensor noise | 2.5 nm rms |

From these basic requirements the following detailed requirements were derived when the needs of the ACS were also included. These derived requirements formed the basis of the design of the production sensors. Performance testing of sensors has been performed on production prototype units and a sample of the production run. The results are summarized below:

| | ACS DERIVED REQUIREMENTS | MEASURED PERFORMANCE |
|---|---|---|
| SYSTEM REQUIREMENTS | | |
| sensor "noise" | 2.5 nm rms | 1 nm rms |
| measurement precision | 3 nm lsb | 3 nm lsb |
| dynamic range | ± 12 µm | ± 12 µm |
| temporal drift | 6 nm/wk | 3.2 nm/wk (system) |
| temperature effects | < 3 nm/°C | 2 nm/°C (system) |
| operating range | 2 °C ± 8 °C | ok |
| physical protection | boot | ok |
| MECHANICAL REQUIREMENTS | | |
| gravity | 9 nm rms - after correction | 7.5 nm rms - after correction |
| temporal drift | 3 nm/wk | 3.2 nm/wk (system) |
| temperature effects | < 3 nm/°C | 1.5 nm/°C |
| mass | < 3 kg | 2 kg |
| servicability | for mirror removal | ok |
| intersegment motion | 4.6 nm rms - after correction | 4.5 nm rms - after correction |
| offset | < ± 160 µm | < ± 180 µm |
| ELECTRONIC REQUIREMENTS | | |
| power | < 2 W | < 0.5 W |
| noise | < 2.5 nm rms system | < 0.5 nm rms |
| electronic stability | < 3 nm/wk | 0.3 nm/wk |

## APPENDIX B

### Physical Characteristics

The sensors are made of the same grade of Zerodur as the primary mirror segments. Zerodur was chosen for its dimensional stability, low temperature coefficient, machineability and coatability. Attachment hardware is of stainless steel, spring steel, brass and invar. The sizes and weights of the various pieces are:

SENSOR DIMENSIONS

| | | | |
|---|---|---|---|
| Paddle assembly | | | |
| | drive base | 45.2 x 50 x 24mm | 115 gms |
| | drive paddle | 140.3 x 50 x 23mm | 404 gms |
| | force plate | 45.2 x 50 x 24mm | 123 gms |
| | | | 642 gms |
| Sense assembly | | | |
| | sense base | 45.2 x 50 x 10 mm | 47 gms |
| | bottom sense | 99.2 x 50 x 10 mm | 125 gms |
| | sense spacer | 45.2 x 50 x 31 mm | 149 gms |
| | top sense | 99.2 x 50 x 10 mm | 125 gms |
| | force plate | 45.2 x 50 x 24 mm | 123 gms |
| | | | 569 gms |

With the boot, attachment hardware and front end electronics installed, each half of the sensor mounted on the mirror segment weighs – 1 kg.

## APPENDIX C

### Fabrication Techniques

Parts were fabricated by grinding and drilling using diamond tools and slurry abrasives. Parts were fabricated by an optical house that combined machine shop grinding techniques with optical slurry grinding techniques to achieve dimensional tolerances for flatness and parallelism of 1 μm with thickness tolerances of 10 μm. Polishing and etching were used for stress relief. Typical fabrication requirements were:

| | |
|---|---|
| size | ± 0.13 mm |
| flatness | ± 0.001 mm |
| coplanarity | 0.002 mm |
| profile | 0.001 mm (spherical baseplate surface) |
| thickness | ± 0.010 mm |
| surface finish | 5 μm in critical areas |

A ground surface for coated Zerodur parts was chosen on the basis of previous experience with coating adhesion on Zerodur. Electrically conductive coatings are sputtered gold (2.5 μm) over a binding layer of chrome. The coating adhesion of the production pieces exceeds the strength of the Zerodur. Production sample coatings are routinely tested by soldering copper wires to the coating and then pulling divots of Zerodur from the surface.

Patterns that form the capacitor areas (30 x 30 mm) are created using a normal photoetching technique. Coating and pattern fabrication requirements are shown below:

| | |
|---|---|
| material | gold (99.9% or better) |
| thickness | minimum 1.0 μm (2.5 in practice) |
| resistance | < 0.1 Ω per square |
| coverage | to conform to edges and to tapered holes |
| uniformity | 20% face to face; 50% sides to ends |
| pattern | resistance between sense area and surrounding ground coating 20 MΩ or greater. Uniformity of sensor area to be better than 0.2% |

Analog signals are carried on standard coaxial cable connected to the coated areas of the sensors using low melting point indium solder to minimize the risk of permanent damage to Zerodur parts.

The protective boot is vacuum formed plastic and is mounted using resilient adhesive to control temperature induced bending of the mirror segment. The Bellows is molded silicone rubber and is intended to exert no more than 50 gms force on the segment edge under normal operation.

# END

# DATE FILMED

12/14/90